Jinst

Published by IOP Publishing for Sissa Medialab

Received: *December 27, 2021*
Revised: *February 21, 2022*
Accepted: *March 1, 2022*
Published: *March 24, 2022*

TECHNICAL REPORT

DOI correction for gamma ray energy reconstruction based on energy segment in 3D position-sensitive CdZnTe detectors

Y. Li,[a] P. Gong,[a,b,*] X. Tang,[a,b] Z. Hu,[a] P. Wang,[c] F. Tian,[a] S. Wu,[a] M. Ye,[a] C. Zhou[d] and X. Zhu[d]

[a] *Department of Nuclear Science and Technology, Nanjing University of Aeronautics and Astronautics, Nanjing 211106, China*
[b] *Key Laboratory of Nuclear Technology Application and Radiation Protection in Astronautics, Ministry of Industry and Information Technology, Nanjing 211106, China*
[c] *School of Environmental and Biological Engineering, Nanjing University of Science and Technology, Nanjing 210094, China*
[d] *Jiangsu Nuclear and Radiation Safety Supervision and Management Center, Nanjing 210019, China*

E-mail: gongpin@nuaa.edu.cn

Abstract: The amplitude of the induced signal in 3D CdZnTe detector depends on the depth of interaction (DOI). Therefore, calibrating the detector by using DOI correction technology plays a crucial role in improving the energy resolution of the detectors to gamma rays. The current DOI correction method focuses on the single energy gamma rays, and its application to multiple energy gamma-rays are not found. In this study, we propose an improved energy correction algorithm with excellent correction results in the multiple energy gamma-ray detection. In the experiment, the DOI correction factors of a CdZnTe detector under different energies are discussed. The energy resolution and peak height of multiple energy peaks in the energy spectrum are significantly improved by using the segment energy correction method. We also extend the DOI correction method to the gamma detectors used in the Compton imaging, and the influence of this method on the Compton imaging quality is also discussed. For a single ^{60}Co point source, the intrinsic efficiency increases from 6.5‰ to 8.3‰.

Keywords: Gamma detectors; Gamma detectors (scintillators, CZT, HPGe, HgI etc); Imaging spectroscopy

*Corresponding author.

https://doi.org/10.1088/1748-0221/17/03/T03004

2022 JINST 17 T03004

Contents

2022 JINST 17 T03004

1 Introduction

Three-dimensional position-sensitive CdZnTe (3D CdZnTe) semiconductor detectors are widely applied in spectroscopic and imaging fields [1–3]. The Orion group at the University of Michigan developed a CdZnTe detector used for γ spectroscopy with an excellent energy resolution [4]. In addition, the 3D CZT detectors have gamma ray and neutron imaging capabilities [5–7]. They have been utilized in the Compton imaging and coded aperture imaging technology [8–13]. The 3D CdZnTe detectors have been successfully utilized to develop Compton cameras which were applied in the homeland security [14, 15] and the exploration of the universe [16, 17].

The energy resolution is a critical parameter for the CdZnTe detectors used not only in the gamma spectroscopy but also in the Compton imaging. The energy information of incident gamma rays dominates the calculation accuracy of the scattering angle and the judgment of the sequence of events in the Compton imaging. There are many factors that infect the energy resolution of CdZnTe detectors, such as the electron trapping, weighting potential on both sides of detectors, the nonuniformity of the material, and the electronic variation [18]. The deposited energies in the detector also vary with the depths at which the gamma ray interacts in the crystal. The response of a particular CdZnTe detector to the gamma rays of a certain energy thus consists of a single energy peak and a low energy tail below. In order to improve the energy resolution, some researchers proposed a DOI correction method which could give the energy of the incident mono-energetic gamma rays by using the relationship between the depth and signal amplitudes caused by deposited energy and thereby effectively improve the energy resolution of the detector.

In previous studies, DOI correction is only for the radioactive sources with a single energy peak [5, 19–21]. Calibration of sources with multiple energy peaks is rarely discussed. However, in

the research of space exploration and medical imaging [16, 17, 22–24], continuous energy and multi-energy photon imaging are often required, and the current DOI correction is difficult to be applied to this situation. Therefore, developing new DOI correction methods applicable to the multiple energy gamma rays is necessary. Here, we explore the correction factors varying with depth under different gamma ray energies. A depth correction method with energy segments is proposed and applied to the 3D CZT detector. The capability of this method was evaluated by investigating the improvement of shape of the energy spectrum with a variety of peaks. Furthermore, the improvement of energy segment correction on Compton imaging is evaluated and analyzed.

2 Materials and methods

2.1 Calculate the interaction depth

A $22 \times 22 \times 15\,\mathrm{mm}^3$ 3D CdZnTe detector from Kromek (UK) was used in this study. The detector was fabricated with a common planar cathode and 11×11 pixelated anode pads. Each $1.975\,\mathrm{mm} \times 1.975\,\mathrm{mm}^2$ pixel pads is at 2 mm pitch. The detector was operated with the cathode biased at −3000 V. An HPL v1.3 application-specific integrated circuit (ASIC) readout system was used to measure the waveform signals and trigger signals of all channels. The ASIC was optimized for large dimension pixelated CZT sensors, and it measures the energy and timing of signals from 121 anodes and one cathode [10, 25–27]. The 3D CdZnTe detector collected the events generated by the sources located 2 cm above the cathode for calibration.

The interaction depth (d) was inferred by calculating the electron cloud drift time on the basis of the time difference between the signals of the cathode and the anode [28]. The signal induced in the anode was subjected to the small-pixel effect, remaining negligible until the electrons are at approximately one pixel pitch from the anode [29]. A strong current was then induced in those anodes that collect the charge. Different from the anode, the signal induced in the cathode, a planar electrode, started at the time of interaction. Therefore, the electron cloud drift time t can be calculated from the time difference between the cathode signal and the anode signal. The distance between the interaction position and the cathode $z(t)$ can be calculated by eq. (2.1) [30]

$$z(t) = d - \frac{\mu \cdot V}{d} \cdot t \tag{2.1}$$

Where μ is the mobility of electrons ($1000\,\mathrm{cm}^2/\mathrm{V{\cdot}s}$), V is the detector bias, and d is the detector thickness. Figure 1 shows the relationship between the detected energy on the anode and the depth when the detector detects the ^{137}Cs source. The peak position of the huge peak near the cathode (0 cm) is at 662 keV. However, the peak position drops significantly with the increase in depth. The difference in peak position at different depths results in poor energy resolution.

2.2 Calculate the correction factors

Obtaining the correction factors under different energies is necessary before performing the energy segment DOI correction. Five types of radiation sources (350 kBq ^{133}Ba, 420 kBq ^{152}Eu, 210 kBq ^{22}Na, 40 kBq ^{137}Cs, 8.9 kBq ^{60}Co) were used to cover the energy range from 356 keV to 1332 keV. The volume subtended by each pixel is artificially subdivided into depth boxes, and the space in each box is called a voxel. Single-pixel events can be placed into 3D voxels because the anode

2022 JINST 17 T03004

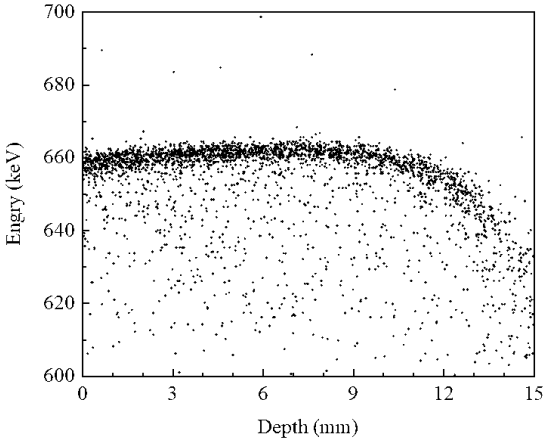

Figure 1. Relationship between the photopeak centroids of 662 keV and the depth under the center pixel of the detector.

channel encodes a unique 2D position. Each pixel is divided into 15 voxels, and each voxel is 1 mm depth. The radioactive sources are placed above the cathode of the detector, and each radioactive source is measured for 2 h. The detection time must be sufficiently long to ensure the accuracy of the calibration. In our experiment, each voxel had more than 200 events.

In accordance with the data readout of the detector, the photopeak centroids of the energy spectrum composed of events within each voxel are obtained. A polynomial P is used to fit the relationship function between the photopeak centroids of each pixel and depth z. In the fitting, the P with an order of 4 is used. The fitting result of the polynomial of order 5 differs very little from that of order 4, and polynomials of higher order may lead to overfitting. The correction factor K of the corresponding energy can be calculated by dividing characteristic energy S of the radioactive source with the relation function P. The calculation of the correction factors for each pixel is expressed as follows:

$$P = a_1 z^4 + a_2 z^3 + a_3 z^2 + a_4 z^1 + a_5 \,, \tag{2.2}$$

$$K = \frac{S}{P} \,. \tag{2.3}$$

The correction factors for 6 types of characteristic energies (344, 356, 511, 662, 1173, and 1332 keV) can be obtained. Figure 2 records the peak position function and correction factor of the central pixel of the detector at different energies. Figure 2(a) shows that the changing trends of the six photopeak centroids P are rising first and then falling, whereas figure 2(b) shows the opposite.

Figure 2(a) shows that as the depth increases, the P value under various energies first rises slowly, and then drops quickly. Only consider the induced charge of the electron calculated by the weight potential. The curve should decrease monotonically. However, there is the effect of electron trapping. For DOI far from the anode, the long electron drift distance more likely to results in electron trapping. Therefore, there is an upward trend on the left side of the curve. The signal drop near the anode is attributed to majorly the non-zero weighting potential. Figure 2(b) records the correction factor K at different energies, which is reciprocal to P. At the same depth, the K value

2022 JINST 17 T03004

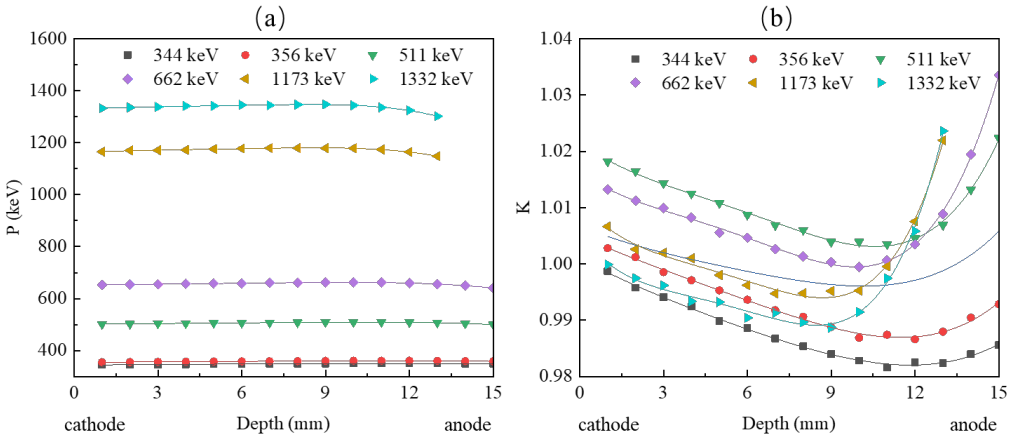

Figure 2. Photopeak centroids P of each voxel (a) and correction factor K (b) as functions of the depth in the central pixel of the detector.

of different energies is different. Therefore, the effect of depth correction is closely related to the selection of characteristic energy S. For HPL v1.3 ASIC, the cathode's timing can be measured by using the threshold crossing of a fast-shaped signal. The voltage signal at the output of the charge amplifier is a ramp with a slope proportional to the energy and inversely proportional to the depth of interact [25]. That's probably the main reason for the influence of energy on the correction factor.

2.3 Energy segment correction

In accordance with the above experiment, six correction factors were obtained, and the depth correction formula was segmented based on the initial energy. Eq. (2.4) shows the correction formula and segmented range of this study. The selected energy ranged from 0 MeV to 1.4 MeV, and the entire range was divided into six energy intervals. Only the correction factor of 356 keV was selected for the energy range below 400 keV because the correction factor K_{344} and K_{356} was extremely close. There is a large difference between K_{511} and K_{356}, and it will cause the energy spectrum deformation at the junction of the energy range. Therefore, in the 370 to 500 keV range, a transition equation is added to improve the distortion of the spectrum. Therefore, in the range of 370 to 500 keV, a transition equation is added to improve the distortion of the energy spectrum, which is based on K_{356} and K_{511}. The 3D-CZT detector can detect the initial energy E_0 of each event. E_0 is used in the correction formula of the corresponding energy range to obtain the corrected energy E_c.

$$E_c = \begin{cases} K_{356} \times E_0 & (0 \le E_0 < 370\,\text{keV}) \\ E_0 \times \left(K_{356} + \frac{(K_{511}-K_{356})\times(E_0-356)}{(511-356)} \right) & (370 \le E_0 < 500\,\text{keV}) \\ K_{511} \times E_0 & (500 \le E_0 < 600\,\text{keV}) \\ K_{662} \times E_0 & (600 \le E_0 < 1000\,\text{keV}) \\ K_{1173} \times E_0 & (1000 \le E_0 < 1300\,\text{keV}) \\ K_{1332} \times E_0 & (1300 \le E_0 < 1400\,\text{keV}) \end{cases} \tag{2.4}$$

2022 JINST 17 T03004

3 Results and discussions

3.1 Spectral performance of single-pixel events

The energy spectrum experiment of a variety of single radioactive sources was performed. Here, only single-pixel events from Compton scattering or photoelectric absorption were selected, and the energy spectra were calibrated with the 344, 356, 511, 662, 1173, and 1332 keV peaks of the sources. Figure 3 shows the total energy spectrum obtained by using different correction methods for the 662 keV peak. Huge differences were found in the energy spectrum results using different correction factors. The K_{662} correction factor was used to obtain the best energy spectrum results with the sharpest peak shape and the highest peak, and the low energy tailing was removed. The energy peaks obtained by other correction factors were significantly lower than K_{662}, and the correction results were poor. When correction factors K_{344} and K_{356} were applied to the 662 keV data, the resolution of the energy spectrum was lower than the energy spectrum before correction, and their peak position had obvious deviation. In addition, segmental correction can also obtain excellent correction results. In the energy range of 500–750 keV, the results of segmented correction and K_{662} correction factor were the same.

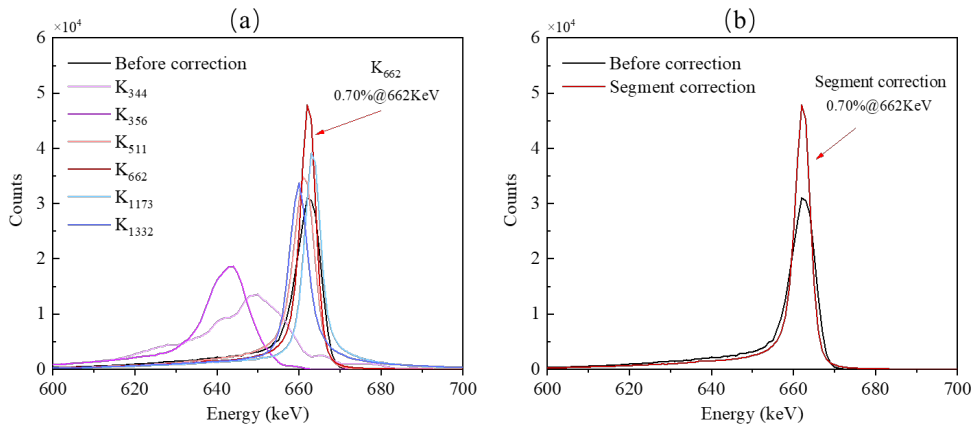

Figure 3. ^{137}Cs spectra of single-pixel events from all pixels after single energy correction (a) and segment correction (b).

Tables 1 and 2 summarize the energy resolution and peak height of each correction method after correction, respectively. Segmented correction significantly improved the performance of all peaks, which obtained the best FWHM and the highest peak height of 356, 511, 662, and 1332 keV. Table 1 shows that segment correction improved the FWHM of 344,356, 511, 662, 1173 and 1332 keV to 1.28%, 1.10%, 1.13%, 0.87%, 0.84% and 0.79%. From table 2, segment correction increased the peak height by over 50% for all peaks. The FWHM and peak height of the segmented corrected energy spectrum at 344 keV were slightly worse than best result. For the correction of 344 keV energy, K_{356} correction factor used in segment correction, which is slightly less accurate than the K_{344} factor in correcting the energy around 344 keV. The segment correction method is proved to be suitable for γ-rays in the energy range of about 356–1332 MeV, but the correction effect is more significant in the low energy range and relatively weak in the high energy range.

2022 JINST 17 T03004

Table 1. Energy resolution full width at half maximum (FWHM) of the total energy spectra for different measurements and reconstructions.

	FWHM@ 344 KeV	FWHM@ 356 KeV	FWHM@ 511 KeV	FWHM@ 662 KeV	FWHM@ 1173 KeV	FWHM@ 1332 KeV
Before correction	2.20%	1.98%	1.84%	1.23%	1.05%	1.07%
Segment correction	**1.28%**	**1.10%**	**1.13%**	**0.87%**	**0.84%**	**0.79%**
K_{344}	1.22%	1.32%	2.73%	2.65%	1.98%	3.95%
K_{356}	1.28%	1.10%	2.14%	2.08%	1.74%	1.79%
K_{511}	2.46%	2.18%	1.13%	1.12%	1.00%	1.09%
K_{662}	3.45%	1.90%	1.25%	0.87%	0.94%	1.26%
K_{1173}	5.10%	3.96%	3.71%	1.01%	0.84%	0.90%
K_{1332}	5.90%	4.07%	4.59%	1.17%	0.87%	0.80%

Table 2. Peak height of the total energy spectra for different measurements and reconstructions.

	344 KeV	356 KeV	511 KeV	662 KeV	1173 KeV	1332 KeV
Before correction	177694	318801	391744	18934	4735	3062
Segment correction	**289837**	**530030**	**614470**	**54556**	**7022**	**4571**
K_{344}	297769	512479	292240	13545	1907	2338
K_{356}	289714	530030	307840	14002	2972	2986
K_{511}	155084	279760	614470	25048	4515	2805
K_{662}	115390	195010	397179	54556	4933	3835
K_{1173}	85152	139543	224269	20274	7021	3444
K_{1332}	82570	133845	200175	17150	6920	4578

A combination of multiple radioactive sources of ^{133}Ba, ^{22}Na, ^{137}Cs, and ^{60}Co was used for energy spectrum measurements. Figure 4 shows the results of energy spectrum after different correction methods. In the energy spectrum corrected by the factor K_{662}, the peak height and the FWHM of the 662 keV were significantly improved, but the peak height and the energy resolution of the 356 keV was significantly reduced. Similarly, the K_{1332} factor effectively improved the energy resolution and peak height of 1173 and 1332 keV, whereas those of other peaks were reduced. The single energy correction only corrected the energy near the *S* value rather than a wide range of energies. In the energy spectrum obtained by segment correction, the peak values and energy resolution of the five energy peaks significantly improved. The segmented correction accurately corrected the event energy of multienergy peaks in a large range.

3.2 Spectral performance of two-pixel events

Multiple anodes are triggered due to the multiple interactions of gamma rays in the 3D-CdZnTe detector and the charge sharing between adjacent pixels. The energy of the two-pixel event was calculated by adding the detected energy values of the two pixels. The reconstructed energy spectra were obtained after correction with different single energy correction factors and segment

2022 JINST 17 T03004

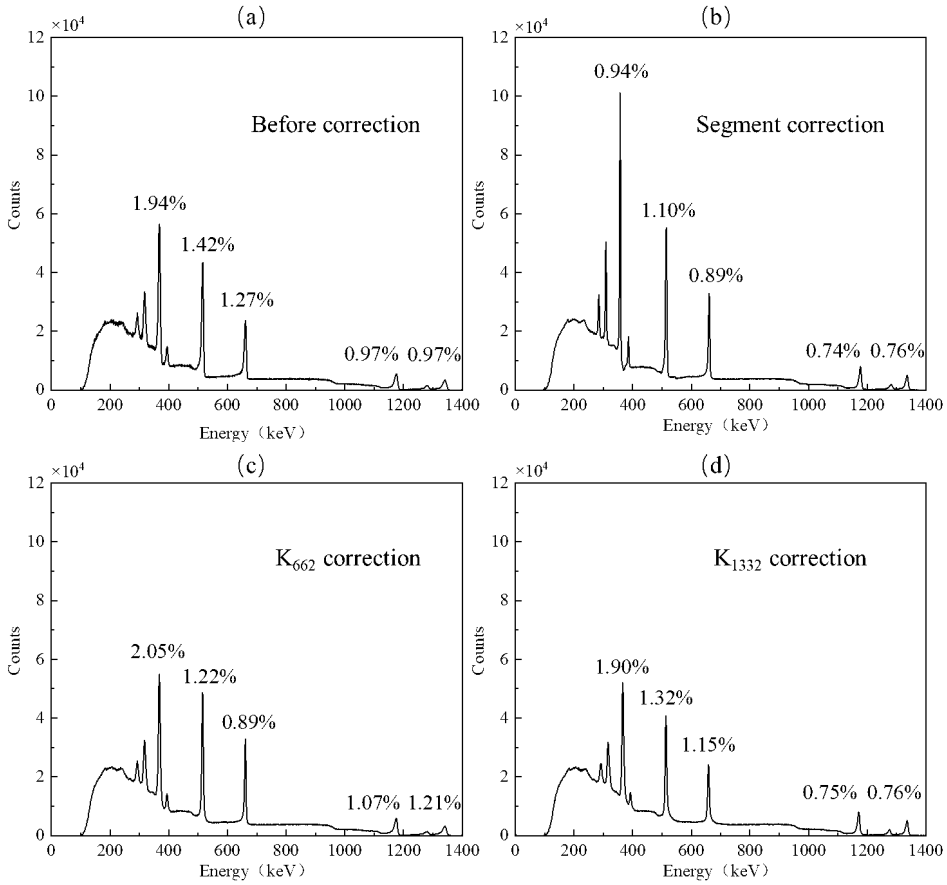

Figure 4. Total energy spectra of multiple sources (^{133}Ba, ^{22}Na, ^{137}Cs, ^{137}Cs, and ^{60}Co) after different correction methods.

correction, as shown in figure 5. The photopeak centroids of the two photo peaks in the original energy spectrum of the two-pixel case were significantly smaller than 1173 and 1332 keV. This condition was due to a charge loss in the interpixel gap, otherwise, a weighting potential crosstalk was found between adjacent pixel electrodes.

Table 3 shows the FWHM and peak height of the energy spectrum obtained after different energy corrections for the two-pixel event. The energy resolution of the 1173 keV peak after segmental correction improved from 3.29% to 2.84%. The energy resolution of the 1332 keV peak increased from 3.81% to 2.97%, which was the best calibration result. The result shows that the segmented correction can optimize the energy of the two-pixel events better than the single energy DOI correction. For the two-pixel events, the energy detected by each pixel is lower than the total energy of the initial photon, which is distributed over a large range.

3.3 Compton imaging experiment

In the Compton imaging experiment, a ^{60}Co point source was placed at a position 11.75 cm above the cathode surface of the 3D-CZT detector, and the imaging time was 20 h. Full 4π imaging can be achieved with a single 3D CdZnTe detector because there is no preference for gamma ray incident

2022 JINST 17 T03004

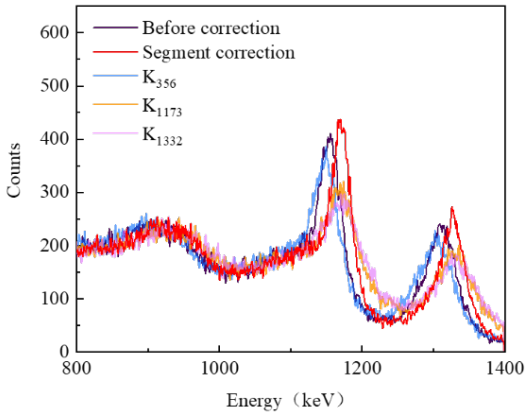

Figure 5. ^{60}Co spectra of two-pixel events from all pixels after different correction methods.

Table 3. Energy resolution FWHM and peak height for different measurements and reconstructions.

	FWHM@ 1173 KeV	Peak height @1173 KeV	FWHM@ 1332 KeV	Peak height @1332 KeV
Before correction	3.29%	416	3.81%	238
Segment correction	**2.84%**	**444**	**2.97%**	**279**
K_{356}	3.82%	398	4.27%	239
K_{1173}	4.65%	326	3.56%	195
K_{1332}	5.22%	313	3.58%	187

from a particular direction. Instead of reconstructing a planar image, the image is reconstructed on the surface of a sphere surrounding the detector as in figure 6 [31]. The two-pixel events were selected for imaging, and the energy window was set from 1300 keV to 1360 keV. The adjacent pixel events were removed as it was not possible to prove if they were charge sharing or Compton events. A simple backprojection algorithm was used to reconstruct the image.

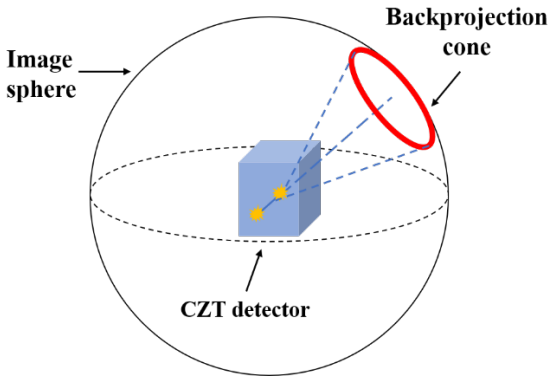

Figure 6. Schematic of detector and imaging plane.

2022 JINST 17 T03004

Figure 7 shows the reconstruction results obtained under different correction methods. The DOI correction has no effect on the position of the reconstructed radioactive source, but the image intensity of the images is relatively different. After segmenting correction, the image intensity at the source location is increased significantly. However, the K_{1332} correction reduces the intensity of the image. This is because that after segmental correction more events can be filtered by energy for Compton reconstruction. In fact, the number of events used for Compton imaging after segmentation correction was 4476, greater than 3935 for the original data and 3492 for K_{1332} correction.

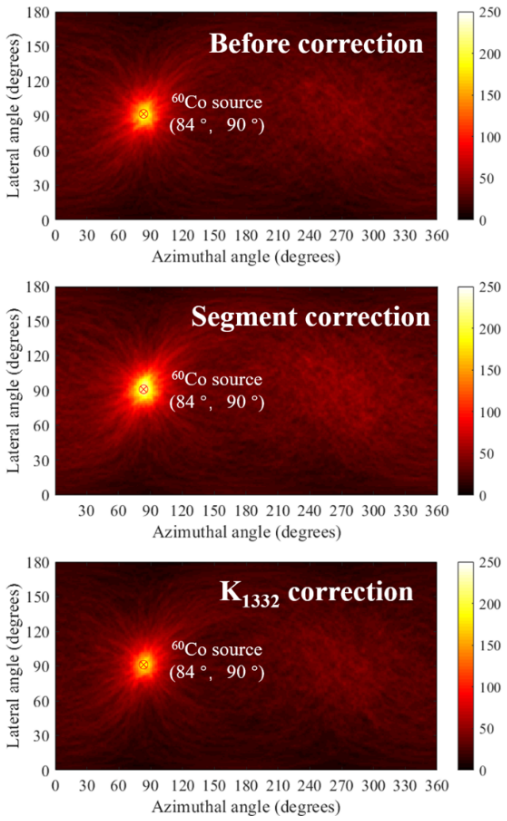

Figure 7. Images of single ^{60}Co source after different correction methods.

The azimuthal slices of the images through the source region are shown in figure 8. Table 3 records the intrinsic efficiency and FWHM of the Compton imaging for different correction methods. The FWHM of the image before correction is approximately 27°, and after segment correction and K_{1332} correction are 26° and 25°, respectively. Therefore, DOI correction will not have a great impact on the image resolution. However, segmentation correction can significantly improve the intrinsic efficiency of the ^{60}Co point source. Intrinsic efficiency is the ratio of radiation interaction events used for image reconstruction to the number of incident radiations. The intrinsic efficiency after segment correction was 8.3‰, much greater than 7.3‰ for the original data, but K_{1332} corrected efficiency dropped to 6.5%. The relative efficiency of the segmented correction results was improved to 113%. This is because after segmental correction, more two-pixel events will pass through the energy window for Compton imaging, while K_{1332} correction will reduce the number of effective events.

2022 JINST 17 T03004

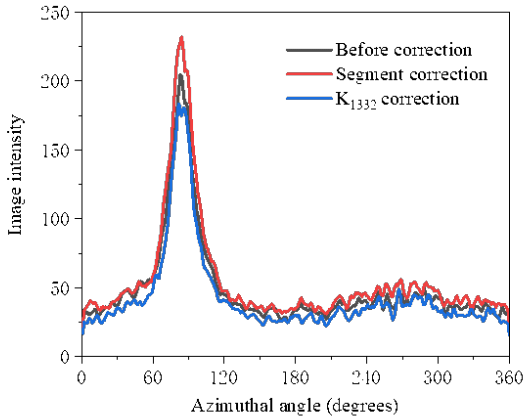

Figure 8. Azimuthal slices of the images shown in figure 7.

Table 4. Intrinsic efficiency and FWHM of the Compton imaging for different correction methods. Relative efficiency refers to the result before relative correction.

	Intrinsic efficiency	Relative efficiency	FWHM
Before correction	7.3‰	100%	27°
Segment correction	8.3‰	113%	26°
K_{1332} correction	6.5‰	89%	25°

4 Conclusions

In this study, the energy spectra of various radioactive sources were measured by using a pixelated CZT detector. The 3D position can be calculated with the data from each channel and drift time measurement. The fluctuation of the detector response in accordance with the interaction position was corrected based on each voxel. The correction factors corresponding to different energies were obtained by detecting different radioactive sources, and a segment correction method based on energy was proposed. In the energy spectrum experiment, single-pixel events and two-pixel events were extracted to reconstruct the energy spectrum. Compared with single energy DOI correction, for single-pixel events with different energies, the energy spectrum corrected by segmented correction has the smallest FWHM and the highest peak height. It is verified that segmental correction has better correction effect for large energy range of events. For the two-pixel events of the ^{60}Co source, the segment correction increased the FWHM of 1332 keV from 3.98% to 3.18%, which was the best calibration result. In the Compton imaging experiment, segment correction improved the intrinsic efficiency when using the ^{60}Co point source in the imaging from 6.5‰ to 8.3‰.

The segment correction method can be used in large volume pixelated CZT detectors with ASIC that can obtain the energy and timing of signals from each channel. In comparison with the traditional DOI correction method used to correct the energy of events, the segmented corrected spectrum has smaller resolution and higher peak height for events with a wide energy range, and simultaneously has a certain improvement in the image intensity of Compton imaging. However, the current experiment is for single-energy Compton imaging, and the subsequent experiment

2022 JINST 17 T03004

for multi-energy Compton imaging will be carried out to verify the generality of the segment correction method.

Acknowledgments

This work was supported by the Primary Research and Development Plan of Jiangsu Province, China (Grant No. BE2019727), the Fundamental Research Funds for the Central Universities, China (Grant No. NT2020017), and the Foundation of Graduate Innovation Center in NUAA, China (Grant No. kfjj20200611).

References

[1] Z. He, G.F. Knoll, D.K. Wehe and J. Miyamoto, *Position Sensitive Single Carrier CdZnTe Detectors*, *IEEE Nucl. Sci. Symp. Med. Imag. Conf.* **1996** (1996) 1.

[2] J.C. Lund, J.M. VanScyoc, R.B. James, D.S. McGregor and R.W. Olsen, *Large volume room temperature gamma-ray spectrometers from CdxZn1 - xTe*, *Nucl. Instrum. Meth. A* **380** (1996) 256.

[3] A. Burger et al., *Defects in CZT crystals and their relationship to gamma-ray detector performance*, *Nucl. Instrum. Meth. A* **448** (2000) 586.

[4] M. Streicher, S. Brown, Y. Zhu, D. Goodman and Z. He, *Special Nuclear Material Characterization Using Digital 3-D Position Sensitive CdZnTe Detectors and High Purity Germanium Spectrometers*, *IEEE Trans. Nucl. Sci.* **63** (2016) 2649.

[5] Y. Kim, T. Lee and W. Lee, *Radiation measurement and imaging using 3D position sensitive pixelated CZT detector*, *Nucl. Eng. Technol.* **51** (2019) 1417.

[6] J. Chu, *Advanced Imaging Algorithms with Position-Sensitive Gamma-Ray Detectors*, Ph.D. Thesis, University of Michigan, Ann Arbor U.S.A. (2018).

[7] S. Brown, *Time-Encoded Thermal Neutron Imaging using Large-Volume Pixelated CdZnTe Detectors*, Ph.D. Thesis, University of Michigan, Ann Arbor U.S.A. (2017).

[8] D.S. Bale and C. Szeles, *Design of High-Performance CdZnTe Quasi-Hemispherical Gamma-Ray CAPture plus Detectors*, *Pros. SPIE* **6319** (2006) 63190B.

[9] X.L. Shen, P. Gong, X. Bin Tang, R. Zhang and J.C. Ma, *Encoding methods matching the* 16×16 *pixel CZT detector of a coded aperture gamma camera*, *Nucl. Sci. Tech.* **31** (2020) 92.

[10] F. Mathy et al., *A Three-Dimensional Model of CdZnTe Gamma-Ray Detector and Its Experimental Validation*, *IEEE Trans. Nucl. Sci.* **51** (2004) 2419.

[11] R. Zhang et al., *Low-noise reconstruction method for coded-aperture gamma camera based on multi-layer perceptron*, *Nucl. Eng. Technol.* **52** (2020) 2250.

[12] A. Shor, Y. Eisen and I. Mardor, *Gamma Spectroscopy with Pixelated CdZnTe Detectors*, *IEEE Trans. Nucl. Sci.* **51** (2004) 1204.

[13] E.G. D'Aillon, M.C. Gentet, G. Montémont, J. Rustique and L. Verger, *Simulation and Experimental Results on Monolithic CdZnTe Gamma-Ray Detectors*, *IEEE Trans. Nucl. Sci.* **52** (2005) 3096.

[14] G. Zentai, *X-ray imaging for homeland security*, *Int. J. Signal Imag. Syst. Eng.* **3** (2010) 1.

[15] Y.L. Liu, J.Q. Fu, Y.L. Li, Y.J. Li, X.M. Ma and L. Zhang, *Preliminary results of a Compton camera based on a single 3D position-sensitive CZT detector*, *Nucl. Sci. Tech.* **29** (2018) 145.

2022 JINST 17 T03004

[16] I. Kuvvetli et al., *A 3D CZT High Resolution Detector for X- and Gamma-Ray Astronomy*, *Proc. SPIE* **9154** (2014) 91540X.

[17] E. Caroli et al., *Development of a 3D CZT Detector Prototype for Laue Lens Telescope*, *Proc. SPIE* **7742** (2010) 77420V.

[18] J. Mann, *Improving Cadmium Zinc Telluride Spectrometer Performance and Capabilities*, Ph.D. Thesis, University of Michigan, Ann Arbor U.S.A. (2016).

[19] W. Lee et al., *Mini Compton Camera Based on an Array of Virtual Frisch-Grid CdZnTe Detectors*, *IEEE Trans. Nucl. Sci.* **63** (2016) 259.

[20] A.E. Bolotnikov et al., *Te inclusions in CZT detectors: New method for correcting their adverse effects*, *IEEE Trans. Nucl. Sci.* **57** (2010) 910.

[21] G. Degeronimo, A.E. Bolotnikov, G. Carini, J. Fried, P. O'connor and S.A. Soldner, *Characterization of an ASIC for CPG sensors with grid-only depth of interaction sensing*, *IEEE Trans. Nucl. Sci.* **53** (2006) 456.

[22] K. Ogane et al., *Simultaneous measurements of single gamma ray of 131I and annihilation radiation of 18F with Compton PET hybrid camera*, *Appl. Radiat. Isot.* **176** (2021) 109864.

[23] S. Motomura, Y. Kanayama, H. Haba, Y. Watanabe and S. Enomoto, *Multiple molecular simultaneous imaging in a live mouse using semiconductor Compton camera*, *J. Anal. At. Spectrom.* **23** (2008) 1089.

[24] M. Sakai et al., *In vivo simultaneous imaging with 99mTc and 18F using a Compton camera*, *Phys. Med. Biol.* **63** (2018) 205006.

[25] G. De Geronimo et al., *Readout ASIC for 3D Position-Sensitive Detectors*, *IEEE Nucl. Sci. Symp. Conf. Rec.* **2007** (2007) 1.

[26] L. Verger, E.G. d'Aillon, O. Monnet, G. Montemont and B. Pelliciari, *New trends in gamma-ray imaging with CdZnTe/CdTe at CEA-Leti*, *Nucl. Instrum. Meth. A* **571** (2007) 33.

[27] G. De Geronimo, A. Dragone, J. Grosholz, P. O'Connor and E. Vernon, *ASIC with multiple energy discrimination for high-rate photon counting applications*, *IEEE Trans. Nucl. Sci.* **54** (2007) 303.

[28] Z. He, W. Li, G.F. Knoll, D.K. Wehe, J. Berry and C.M. Stahle, *3-D position sensitive CdZnTe gamma-ray spectrometers*, *Nucl. Instrum. Meth. A* **422** (1999) 173.

[29] H.H. Barrett, J.D. Eskin and H.B. Barber, *Charge Transport in Arrays of Semiconductor Gamma-Ray Detectors*, *Phys. Rev. Lett.* **75** (1995) 156.

[30] W. Li, Z. He and G.F. Knoll, *A modeling method to calibrate the interaction depth in 3-D position sensitive CdZnTe gamma-ray spectrometers*, *IEEE Trans. Nucl. Sci.* **47** (2000) 890.

[31] D. Xu, Z. He, C.E. Lehner and F. Zhang, *4-Pi Compton Imaging with Single 3D Position-Sensitive CdZnTe Detector*, *Proc. SPIE* **5540** (2004) 144.

2022 JINST 17 T03004